Spring 2020

Strain Components in Friction Stir Extrusion

Megan Ryan

STRAIN COMPONENTS IN FRICTION STIR EXTRUSION

by

Megan Ryan

Bachelor of Science
University of South Carolina, 2019

Submitted in Partial Fulfillment of the Requirements

For the Degree of Master of Science in

Mechanical Engineering

College of Engineering and Computing

University of South Carolina

2021

Accepted by:

Anthony Reynolds, Director of Thesis

Addis Kidane, Reader

Tracey L. Weldon, Interim Vice Provost and Dean of the Graduate School

DEDICATION

To my parents, family, and friends who have been there for me throughout this process, thank you for your support and encouragement.

ACKNOWLEDGEMENTS

Thank you to Dr. Reynolds for his mentorship and guidance throughout this project and throughout my time in graduate school. Thank you to Jeff, Micah, and Kris for their help during this project. This work was performed with financial and technical support from the Pacific Northwest National Laboratory, Lab Directed Research and Development Program, Solid Phase Processing Initiative.

ABSTRACT

Friction stir extrusion is a solid state process that uses a rotating die to perform extrusions. This process can be used to directly recycle waste from machining processes and has been shown to produce wires with desirable mechanical properties. In order to better understand the friction stir extrusion process, the effect of the process parameters on the strain distribution in the wires needs to be understood. The process parameters evaluated in this work are die advance rate, die rotational seed, and die geometry. A total of 16 wires were extruded using different combinations of these process parameters. Marker wires were inserted into the billets prior to extrusion to observe material flow throughout the process. After the extrusion, transvers cross sections were taken at multiple locations along the wires in order to evaluate the strain distribution in each wire. Longitudinal, circumferential, and radial strain were calculated using the change in dimension of the marker wire.

The longitudinal strain was consistent across all wires and was close to the expected value in a conventual extrusion with the same reduction ratio, showing it is not dependent on the process parameters. The radial and circumferential strain were dependent on the process parameters and varied from wire to wire. As the die advance rate per revolution increased, the radial and circumferential strain values began to converge on the expected value for a conventional extrusion with the same reduction ratio. The samples produced with the scroll die had very similar strain distributions when

compared to the samples produced with a flat die and the same process parameters. While the images of the cross sections showed that the scroll die changed the marker wire shape, it did not alter the strain distribution. The sum of the strain components was very close to zero for all cross sections, which is expected in a controlled volume plastic deformation process. This shows that the method used produced accurate strain results.

TABLE OF CONTENTS

Dedication iii

Acknowledgements iv

Abstract v

List of Tables ix

List of Figures x

List of Symbols xiii

Chapter 1 Introduction 1

Chapter 2 Literature Review 4

2.1 Wire Production via Friction Stir Extrusion 4

2.2 Mechanical Properties of wires 6

2.3 Strain in Extruded Wires 7

2.4 Marker Insert Technique 7

Chapter 3 Experimental Procedures 10

3.1 Extrusion Process 10

3.2 Sample Preparation 11

3.3 Strain Analysis 12

Chapter 4 Results and Discussion 16

4.1 Cross Section Images 16

4.2 Strain Components 17

4.3 Effect of Parameters on Strain 20

4.4 Scroll Die..... 25

4.5 Validity of Method..... 32

Chapter 5 Conclusions..... 33

References..... 34

LIST OF TABLES

Table 3.1: The process parameters and die used for each extrusion 12

Table 4.1: Die advance per revolution for each wire 23

LIST OF FIGURES

Figure 3.1: Die geometry of (a) scroll die (b) flat die 10

Figure 3.2: (a) Final area measurement (b) Final length measurement (c) Final average thickness measurement 14

Figure 3.3: (a) Color contrast feature used to measure area of marker wire (b) Arc measurement feature used to measure final length (c) Linear measurement feature used to make measurements to calculate average thickness.....15

Figure 4.1: Images taken on optical Microscope of wire cross sections 100mm from the start of the extrusion. (a) Cross section from wire 1 produced at 4 mm/min and 300 rpm (b) Cross section from wire 2 produced at 8 mm/min and 300 rpm (c) cross section from wire 3 produced at 12 mm/min and 300 rpm (d) cross section from wire 4 produced at 8 mm/min and 150 rpm (e) cross section from wire 5 produced at 8 mm/min and 450 rpm (f) cross section from wire 6 produced at 16 mm/min and 300 rpm (g) cross section from wire 7 produced at 40 mm/min and 300 rpm (h) cross section from wire 8 produced at 40 mm/min and 150 rpm.....16

Figure 4.2: Longitudinal strain in flat die wires as a function of position from the start of the extrusion.....18

Figure 4.3: Radial strain in flat die wires as a function of position from the start of the extrusion.....19

Figure 4.4: Theta strain in flat die wires as a function of position from the start of the extrusion.....20

Figure 4.5: The average strain values of wires extruded with a rotational speed of 300 rpm plotted against the die advance rate used for each extrusion.....21

Figure 4.6: The average strain values of wires extruded with a 8 mm/min feed rate plotted against the rotational speed used for each extrusion.....22

Figure 4.7: The average strain values of wires extruded with a 40mm/min feed rate plotted against the rotational speed used for each extrusion.....22

Figure 4.8: Average strain values as a function of die advance rate per revolution.....24

Figure 4.9: The strain components of extrusion x and extrusion x as a function of distance from the start of the extrusion 25

Figure 4.10: Cross sections from extrusions performed at 300 rpm and 16 mm/min. (a) flat die extrusion. (b) scroll die extrusion 26

Figure 4.11: Cross sections from extrusions performed at 300 rpm and 40 mm/min. (a) flat die extrusion. (b) scroll die extrusion 26

Figure 4.12: Cross sections from extrusions performed at 150 rpm and 40 mm/min. (a) flat die extrusion. (b) scroll die extrusion 27

Figure 4.13: Longitudinal strain in the scroll die samples as a function of distance from the start of the extrusion.....28

Figure 4.14: Theta strain in the scroll die samples as a function of distance from the start of the extrusion.....28

Figure 4.15: Radial strain in the scroll die samples as a function of distance from the start of the extrusion.....29

Figure 4.16: Strain Components of wires extruded at 150 rpm and 40 mm/min with both a flat die and scroll die as a function of distance from the start of the extrusion.....29

Figure 4.17: Strain Components of wires extruded at 150 rpm and 40 mm/min with both a flat die and scroll die as a function of distance from the start of the extrusion 30

Figure 4.18: Strain Components of wires extruded at 300 rpm and 12 mm/min with both a flat die and scroll die as a function of distance from the start of the extrusion 31

Figure 4.19: Strain Components of wires extruded at 150 rpm and 8 mm/min with both a flat die and scroll die as a function of distance from the start of the extrusion 31

Figure 4.20: The sum of the strain components plotted against the distance from the start of wire for all extrusions 32

LIST OF SYMBOLS

ε_l	Longitudinal Strain
ε_θ	Circumferential Strain
ε_r	Radial Strain
A_o	Initial area of marker wire before the extrusion process
A_f	Final area of marker wire post extrusion process
D_o	Initial diameter of marker wire before the extrusion process
c	Average cord length of marker wire before the extrusion process
L	Final length of marker wire in the circumferential direction post extrusion
t	Average thickness of marker wire in radial direction post extrusion

CHAPTER 1

INTRODUCTION

Friction stir extrusion was first developed at The Welding Institute in the 1990's. It was developed from friction processing, a group of operations that utilize friction as a thermal mechanical energy source for the welding and reprocessing of metals by plasticizing a specific region [1]. Friction stir extrusion was derived from friction stir welding, which was invented in 1991 by Wayne Thomas at The Welding Institute [2]. Friction stir welding is a solid-state process that joins metals through intense plastic deformation. Friction stir wielding is ideal for joining lightweight metals such as Aluminum, magnesium and titanium, as well as for joining dissimilar metals [3]. These principals were applied to extrusion to create friction stir extrusion, which was patented by the Welding Institute in 1993 [4].

Similar to traditional extrusion, FSE changes the shape of the extrusion charge by forcing the material through a die. In FSE the die rotates as it plunges into the chamber of material, producing friction between die surface and the material to be extruded. This creates intense plastic deformation and as the temperature increases the material begins to flow through the die. Friction stir extrusion can be used to produce wire, rods with circular and square cross sections, and hollow tubes.

Friction stir extrusions are either rate controlled or force controlled. In rate controlled extrusion, the die advance rate is held constant and the extrusion force varies throughout the extrusion. As the extrusion progresses and the process temperature

increases, the force required to maintain the controlled extrusion rate decreases. In force controlled extrusion, the extrusion force is held constant throughout the extrusion and the rate changes. As the extrusion temperature increases throughout the extrusion, the extrusion rate also increases. In addition to either extrusion rate or extrusion force, the rotational speed of the die and the geometry of the die are also controlled variables. The response parameters during the process are the extrusion temperature, the power required, and the torque required to perform the extrusion.

After it was patented in 1993, the technology was not explored further for many years. It began to receive attention again due to its potential as a recycling method for waste produced from machining processes. Recycling the waste from these processes prevents valuable material from being discarded, in turn reducing the need for new raw material. Currently, 25% of the worlds CO2 emissions come from material production, and the demand for materials continues to increase each year [5]. In order to meet material demands and reduce negative environmental impact of the material industry, there has been increased interest in recycling as a solution. Traditional recycling methods involve re-melting and re-casting materials. This process is highly energy intensive and results in material loss. In addition, this method requires additional manufacturing processes in order to produce a final product. While these traditional recycling process offer environmental benefits and economic savings over primary production, a more energy efficient recycling process would offer further benefits.

Friction Stir Extrusion is a solid state process that does not require the material to reach its bulk melting point. Fully melting materials is a very energy intensive process, so by allowing the extrusion to occur at a solid state the overall energy consumption of the

recycling process can be greatly reduced. FSE has been shown to produce a 53% reduction in primary energy demand compared to recycling through re melting [6]. FSE is able to produce wire directly from machining chips or a solid billet, simplifying the multi-step traditional recycling process into one convenient process. FSE saves material and energy compared to traditional extrusion, producing cost savings as well as a reduced environmental impact. While FSE shows promising benefits, the process needs to be better understood. Specifically, the effect of the chosen process parameters needs to be better understood. This work explores the effect of the process parameter on the resultant strain distribution in friction stir extruded wires.

CHAPTER 2

LITERATURE REVIEW

2.1 WIRE PRODUCTION VIA FRICTION STIR EXTRUSION

Many manufacturing processes produce material waste, and there is high economic incentive to recycle and reuse this material. Machining chips have traditionally been difficult to recycle due to their high surface to volume ratio. Friction stir extrusion has been utilized to extrude wire directly from these machine chips left over from other manufacturing processes. Magnesium alloys are popular in many industries due to their high specific strength and great machinability [7]. Due to its common use, there are large volumes of magnesium alloy chips produced that need to be recycled. Wires have been extruded directly from mg alloy machining chips using FSE [8]. Using rate controlled extrusion with a die advance rate of 14mm/min and a die rotation rate of 250 rpm, Ansari et al. were able to produce wires 15 - 20 mm in length with no visible surface defects. The wires had a higher mechanical strength than the parent material. Wires have also been successfully extruded from AZ31 Mg machining chips [9]. Buffa et al. produced wires with rate controlled extrusion with a feed rate of 30 mm/min and varied die ration rate. The best results were obtained with a rational speed of 700 rpm, which produced a defect free wire with a tensile strength 80% of the parent material.

Aluminum is another material with high strength to density ratio, making it an important material in the aerospace and automotive industries. Due to its common use in these industries, considerable amounts of aluminum chips are produced. FSE had been

successfully applied to the direct recycling of aluminum alloy chips. Tang and Reynolds extruded wires from both AA2050 and AA2195 aluminum chips [10]. The wires produced from these alloys were intended to be used as a welding consumable and in wire arc additive manufacturing. They were extruded with a constant extrusion force of 17.8 kN and rotational speeds ranging from 100 rpm to 400 rpm. Low rotational speeds generated the lowest amount of heat and cold cracking was present along the length of the wire produced at 100 rpm. High rotational speeds were shown to produce excessive heat and the wire produced at 400 rpm had hot cracks on the surface. The intermediate rotational speeds ranging from 150 rpm to 350 rpm were proven to produce defect free wires for both of the tested alloys. FSE has also been applied to AA7277 aluminum chips [11]. Behnagh et al. utilized a constant extrusion force of 1.8 kN with the die rotation speed ranging from 90 rpm to 250 rpm. They also found that wires produced with intermittent rotational speeds were the most successful due to the fact that their surface were not impacted by cold tearing or hot cracking. Tensile tests performed on the defect free wires showed they had mechanical properties very close to the parent material.

Friction stir extrusion has also been proven as an effective method to produce wire directly from powder. Whalen et al. produced aluminum rods from Al-12.4TM powder [12]. The friction stir extrusion method was able to consolidate the power and extrude the rods all in one process. They were able to produce 5 mm diameter rods that had a higher elongation than rods of the same material that were conventionally extruded. Bafarri et al. mixed a silicon carbide micro powder into AA2024 aluminum chips and were able to successfully extrude defect free wires from the mixture [13]. This work showed that friction stir extrusion can be used as a fabrication method for metal matrix composites.

Friction stir extrusion has also been proven as a successful method to produce wires from solid billets. Wires were able to be produced form a 2050 aluminum billet using a scrolled die and force controlled extrusion [14]. Baffari et al. were able to produce sound wires 300mm in length, to be used as base material for wire arc additive manufacturing. These works show the feasibility of creating good quality wire through friction stir extrusion.

2.2 MECHANICAL PROPERTIES OF WIRES

Friction stir extrusion has been shown to produce wires with improved mechanical properties when compared to traditionally extruded wires. During FSE, the material undergoes high shear deformation, which leads to grain refinement in the final product. In aluminum wires, this refined grain structure leads to an increase in mechanical strength [15]. Ahmadkhanbeigi et al. produced hollow tubes via FSE that showed 23% increase in yield strength when compared to the base material. The refined grain structure of these tubes also produced an increase in microhardness.

The properties of magnesium wires have also been shown to improve through FSE. Behnagh et al. observed dynamic recrystallized grain structure in friction extruded wires produced from Mg chips [16]. All wires produced showed improved mechanical strength and ductility, with the largest improvements occurring in the wire with the most refined grain structure. Sharifzadeh et al. produced wires from Mg chips via FSE and found that the wires had a fine homogeneous grain structure [17]. This grain refinement caused the wires to have improved hardness, strength and corrosion resistance. These improved physical properties show that friction stir extrusion is a valuable manufacturing process that has the ability to produce wires with desirable mechanical properties.

2.3 STRAIN IN EXTRUDED WIRES

In conventional extrusion, strain is governed by the reduction ration (r).

$$r = \frac{A_o}{A_f} \qquad \text{(Eq. 1)}$$

A_o is the initial cross sectional area of the billet and A_f is the final cross sectional area of the extruded part. The true strain (ε) can be calculated by taking the natural logarithm of the reduction ratio.

$$\varepsilon = \ln \frac{A_o}{A_f} \qquad \text{(Eq. 2)}$$

FSE shares many similarities with conventional extrusion, with the significant difference being the rotating die in friction extrusion. This rotating die changes the material flow pattern and changes the strain pattern experienced in the wire. To better understand the FSE extrusion process, the difference in strain between conventionally extruded wires and friction stir extruded wires needs to be understood.

In order to better utilize the friction stir extrusion process to achieve specific results, the effect of the process parameters also needs to be better understood. Process parameters include die rotation rate, extrusion rate, and extrusion force. One property of the wire directly impacted by the process control parameters is the strain pattern. Gaining an understanding of the strain patterns in wires with different combinations of process parameters will allow the optimal parameters to be chosen for wires for specific applications.

2.4 MARKER INSERT TECHNIQUE

In order to measure strain, the marker insert technique is utilized. This technique involves drilling a hole in the billet and inserting a marker wire of a different material prior

to the manufacturing process. By observing the marker wire in the final product, the material flow pattern can be determined.

The marker insert technique was first used to analyze conventional extrusion [18]. Henry Valberg utilized a grid pattern technique to observe material flow in direct axisymmetric extrusion. In order to create the grid pattern, radial and axial holes were drilled in the billet. Indicator wire pins were then inserted into the drilled holes, creating a stripe pattern. After the extrusion, both the wire and the extrusion butt were sectioned in order to observe the transverse and longitudinal marker pins. This grid pattern technique was successful and Valberg was able to develop a model of material flow. Notably, it was successful even in areas with high deformation, which were a shortcoming of previous techniques used.

The marker insert technique has been used to observe material flow friction stir welding [19]. Seidel and Reynolds placed 6 marker inserts in the weld path at varying heights on both sides of the weld centerline. After the friction stir welding process, 0.025 mm thick slices were cut from the top of the weld. The slices were etched in order to create contrast between the AA5454 marker material and the AA 2195 base material. The marker insert technique was successful, and the marker material in these sections was both continuous and distinguishable from the base material. This allowed the material flow in the longitudinal, transverse and vertical directions to be observed and correlated to welding parameters and tool geometry.

Marker wire inserts have also been used in friction stir extrusions [20]. Baffari et al. utilized the marker wire technique and inserted a copper maker wire into the center of a AZ31 Magnesium billet that was compacted from machining chips. The marker wire was

able to successfully show that a helical material flow pattern occurred during the extrusion. Li et al. used an AA2195 marker wire inserted into an AA6061 billet to show that material moved gradually to the center of the extrusion following a spiral path [21]. In addition to mapping material flow, the marker wire technique has also been used to estimate strain in friction stir extrusions. Li et al. used an AA2195 marker wire in an AA6061 billet and tested 2 different rotational speeds and 2 different extrusion forces for a total of 4 tests [22]. It was observed that the spiral pattern of the marker wire decreased along the length of the extrusion, showing that as the extrusion progresses and the extrusion rate increases, it becomes more similar to a traditional extrusion. These tests used force controlled extrusion, which produced varying extrusion rates throughout the extrusion. This made it difficult to correspond strain to specific parameters, and it was determined that in order to produce consistent strain levels the rate of the extrusion needed to be controlled.

CHAPTER 3

EXPIREMENTAL PROCEDURES

3.1 EXTRUSION PROCESS

Wires were extruded using a Shear Assisted Processing and Extrusion (ShAPE) machine at Pacific Northwest National Laboratories. The wires were extruded with rate-controlled extrusion, with a constant feed rate throughout the extrusion. During the extrusions the process temperature, force, power, pressure and torque were recorded. The wires were produced with MP159 (cobalt nickel alloy) dies. The first die was a flat faced die and the second was a scrolled face die. The die geometry can be seen in fig. 3.1

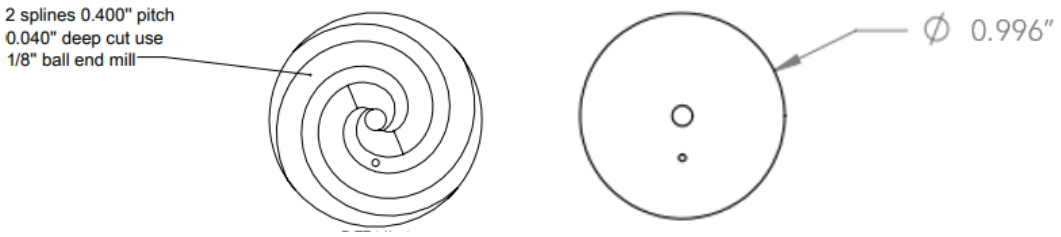

(a) (b)

Figure 3.1: Die geometry of (a) scroll die (b) flat die

The wires were extruded from AA1100 aluminum billets with an initial diameter of 25.4 mm and an initial length of 12.7 mm. A 10:1 reduction ratio was used, creating wires with a final diameter of 2.54 mm. The final length of the extruded wires ranged from 413 mm to 723 mm. In order to measure the strain components, a marker wire was inserted into the billet to track material flow. AA2050 aluminum wire was inserted a distance

equivalent to ⅓ the radius of the billet away from the center of the billet. Some samples also had a marker wire inserted in the center of the billet.

The two extrusion parameters that changed from extrusion to extrusion were die advance rate and die rotation rate. Five die advance rates were tested ranging from 4 mm/min to 40 mm/min. Four die rotation speeds were tested ranging from 150 rpm to 450 rpm. These parameters were combined to create eight different combinations. In addition, two different die were used. Each of the eight conditions was run with both a flat die and a scroll die. The parameters and dies used for each extrusion are detailed in table 3.1.

3.2 SAMPLE PREPARATION

In order to observe transverse cross sections along the extrusion, 2 mm segments were cut from the wires. These segments were cut from the wires at distances ranging from 2 mm to 500 mm from the start of the wire. These segments were mounted in epoxy and ground with silicon carbide paper starting with 120 grit and ending with 1200 grit. The samples were then polished with 5 and 3 micron diameter alumina powder and then finally with colloidal silica. In order to distinguish the AA2050 marker wire from the AA1100 wire, a Keller's etch was used. The Keller's etch was prepared with 190 mL water, 5 mL nitric acid, 3 mL hydrochloric acid, and 2 mL hydrofluoric acid. Keller etch was chosen because it produced good contrast between the AA1100 base material and the AA2050 marker wire, which allowed the marker wire to be observed and measured. The samples were submerged for 15 seconds in the Keller’s etch. Images were then taken of each cross section at 500x magnification with an optical microscope.

Table 3.1: The process parameters and die used for each extrusion

Extrusion	Die Advance Rate	Die Rotation Rate	Die
1	4 mm/min	300 rpm	Flat
2	8 mm/min	300 rpm	Flat
3	12 mm/min	300 rpm	Flat
4	8 mm/min	150 rpm	Flat
5	8 mm/min	450 rpm	Flat
6	16 mm/min	300 rpm	Flat
7	40 mm/min	300 rpm	Flat
8	40 mm/min	150 rpm	Flat
9	4 mm/min	300 rpm	Scroll
10	12 mm/min	300 rpm	Scroll
11	8 mm/min	150 rpm	Scroll
12	8 mm/min	450 rpm	Scroll
13	8 mm/min	300 rpm	Scroll
14	16 mm/min	300 rpm	Scroll
15	40 mm/min	300 rpm	Scroll
16	40 mm/min	150 rpm	Scroll

3.3 STRAIN CALCUALTIONS

The strain in the wire can be broken down into three orthogonal strain components in cylindrical coordinates: longitudinal strain in the direction of the extrusion, circumferential strain in the direction of the die rotation, and radial strain in the radial direction. The three components of strain were calculated based on the change in dimension

of the ⅓ radius marker wire in cylindrical coordinates. The three components of strain are calculated with the following equations:

$$\varepsilon_l = \ln\left(\frac{A_o}{A_f}\right) \quad \text{(Eq. 3)}$$

$$\varepsilon_\theta = \ln\left(\frac{L}{D_o}\right) \quad \text{(Eq. 4)}$$

$$\varepsilon_r = \ln\left(\frac{t}{c}\right) \quad \text{(Eq. 5)}$$

A_o is the initial area of the marker wire, 5.06 mm^2, and A_f is the final measured area. L is the length of the marker wire in the theta direction and t is the average thickness in the radial direction. D_o is the initial diameter of the marker wire, 2.54 mm. c is the average cord of the initial marker wire. These measurements can be seen on a wire cross section cross section in fig. 3.2.

A Keyence optical microscope was used to obtain the necessary measurements. The total area of the marker wire was measured using the color contrast between the AA2050 and the AA1100 created by the Keller's etch. The arc measurement function on the microscope was used to measure the length of the ⅓ radius marker wire since the marker wires showed a spiral pattern. The linear measurement function was used to measure the thickness of the ⅓ radius marker wire spiral at increments along the spiral to determine the average thickness in the radial direction. Figure 3.3 details how each measurement was taken.

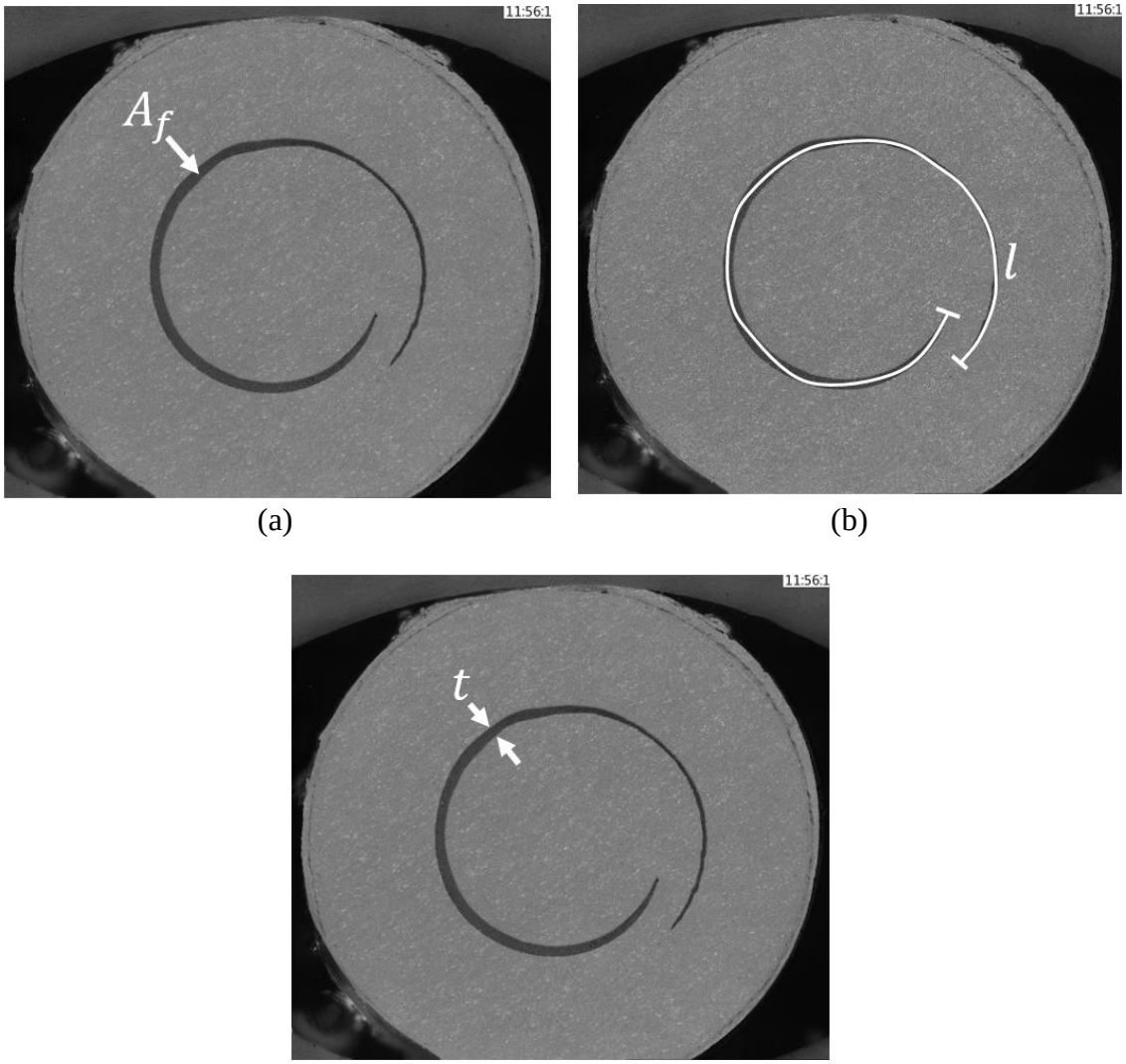

Figure 3.2: (a) Final area measurement (b) Final length measurement (c) Final average thickness measurement

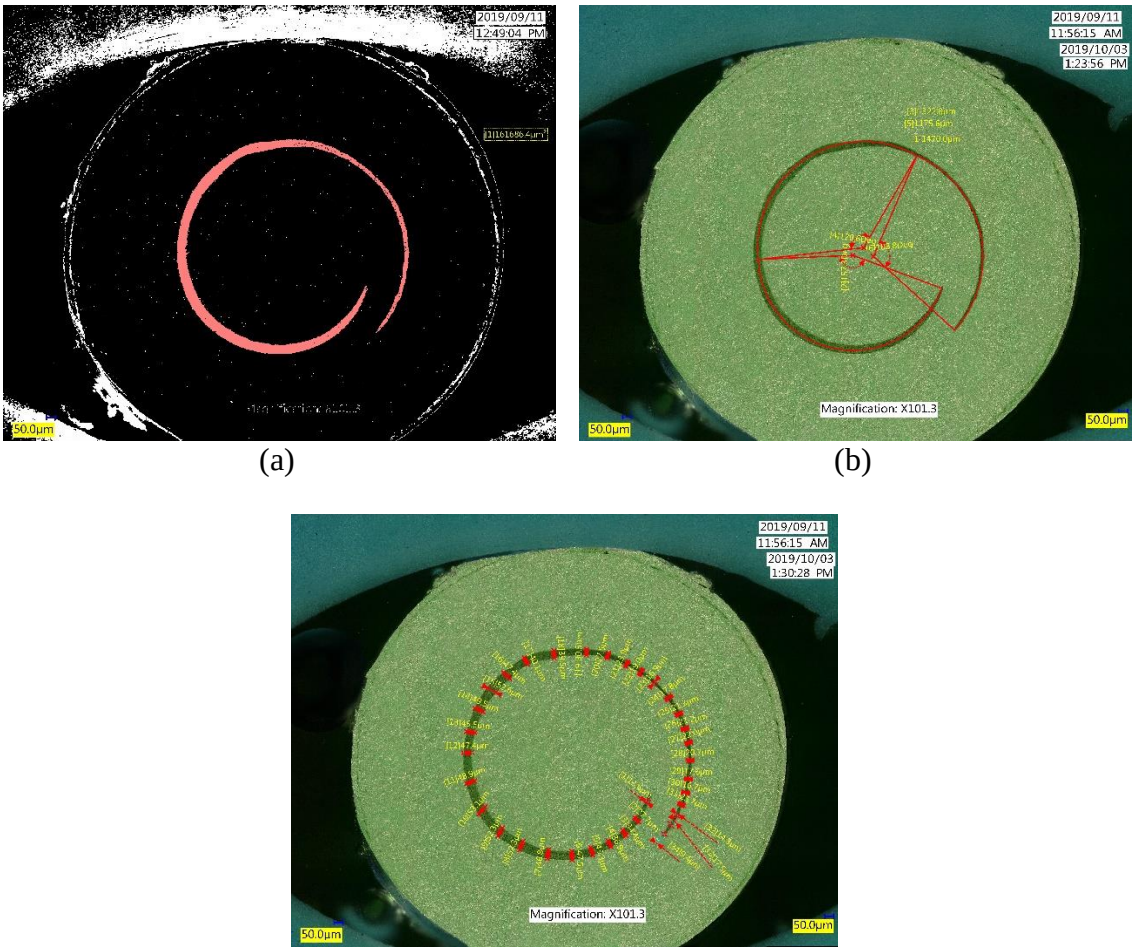

(a) (b)

(c)

Figure 3.3: (a) Color contrast feature used to measure area of marker wire (b) Arc measurement feature used to measure final length (c) Linear measurement feature used to make measurements to calculate average thickness

CHAPTER 4

RESULTS AND DISCUSSION

4.1 IMAGES

The marker wire technique that was utilized proved to be successful. A clearly defined marker wire was visible throughout the wires extruded with a flat die. After etching, the AA2050 marker was clearly distinguished from the AA100 wire. Images of the cross section taken 100 mm from the start of each flat die wire can be seen in fig. 4.1.

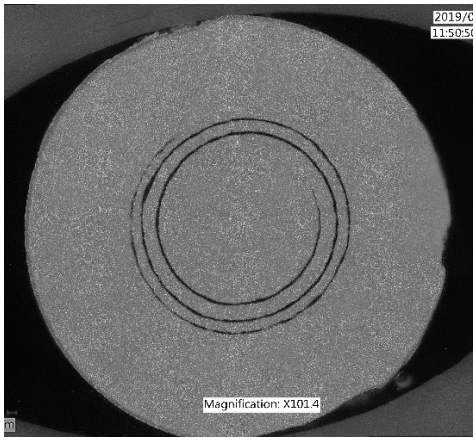

(a)

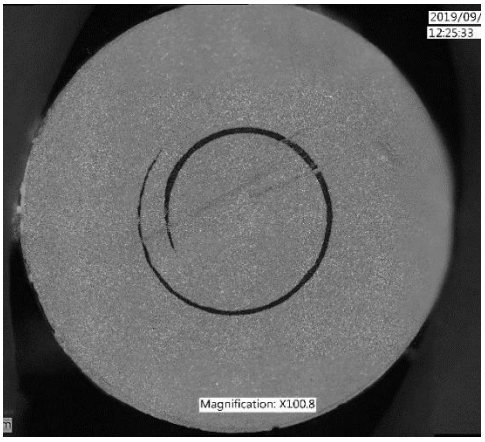

(b)

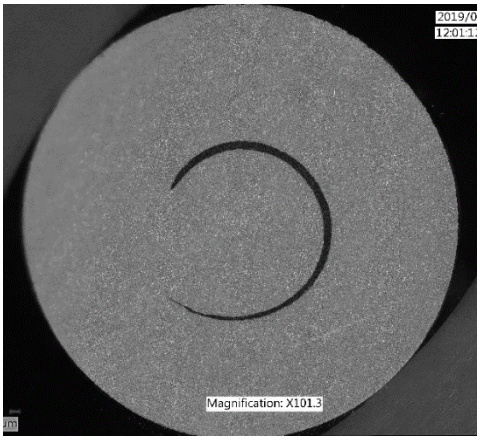

(c)

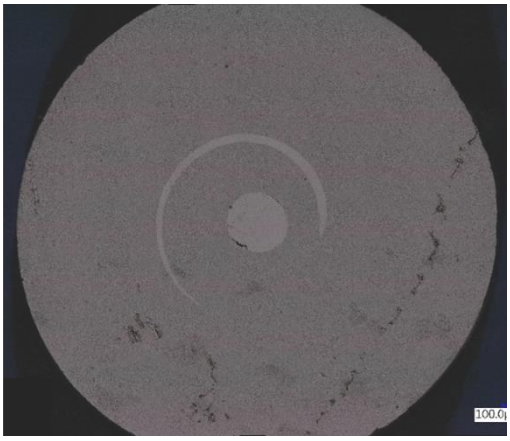

(d)

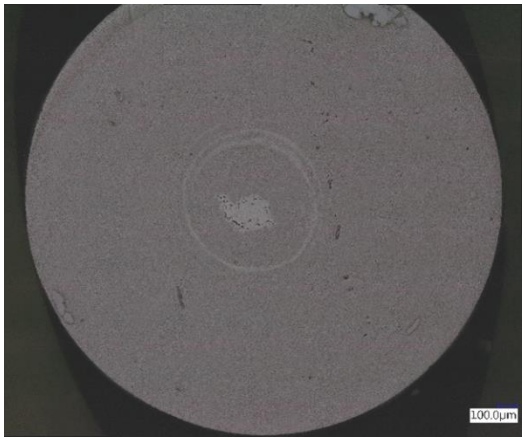

(e)

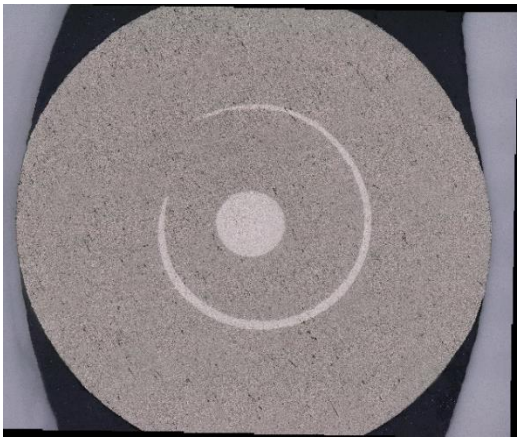

(f)

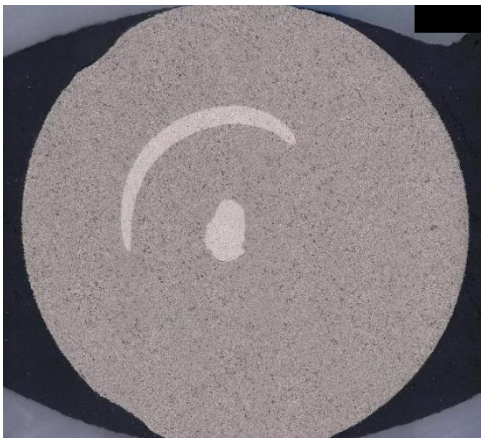

(g)

(h)

Figure 4.1: Images taken on optical Microscope of wire cross sections 100mm from the start of the extrusion. (a) Cross section from wire 1 produced at 4 mm/min and 300 rpm (b) Cross section from wire 2 produced at 8 mm/min and 300 rpm (c) cross section from wire 3 produced at 12 mm/min and 300 rpm (d) cross section from wire 4 produced at 8 mm/min and 150 rpm (e) cross section from wire 5 produced at 8 mm/min and 450 rpm (f) cross section from wire 6 produced at 16 mm/min and 300 rpm (g) cross section from wire 7 produced at 40 mm/min and 300 rpm (h) cross section from wire 8 produced at 40 mm/min and 150 rpm

The pattern of the marker wire varies from sample to sample, showing that the different extrusion parameters created different strain patterns in the wires.

4.2 STRAIN COMPONENTS

The three strain components were calculated for each cross section taken from the wires.

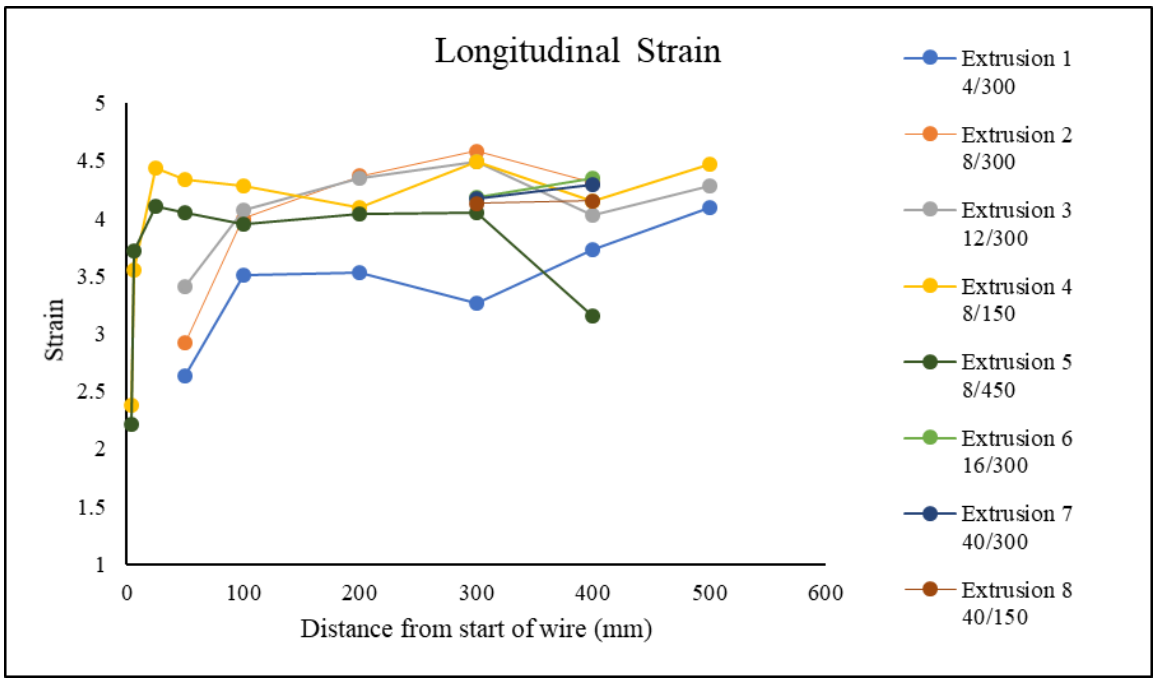

Figure 4.2: Longitudinal strain in flat die wires as a function of position from the start of the extrusion.

Figure 4.2 displays the longitudinal strain observed in the samples extruded with a flat die as a function of position along the wire, measured from the start of the extrusion. The longitudinal strain was lower very close to the start of the extrusion. There was a region corresponding to the beginning of the extrusion where the longitudinal strain increased rapidly. After approximately 100 mm into the wires, the longitudinal strain leveled off and remained constant throughout the rest of the extrusion. This initial region with a rapid change in longitudinal strain could be attributed to the dead metal zone forming at the beginning of the extrusion. Dead metal zones in extrusions can lead to decreased strain [23]. This occurs when material flows only from the center portion of the billet rather than the entire billet feeding onto the extrusion. All the wires with the exception of extrusion 1 experienced similar longitudinal strain values, showing that the extrusion parameters do not affect the longitudinal strain. In a conventional extrusion with a 10:1 reduction ratio,

the expected value of longitudinal strain is 4.6. The longitudinal strain observed in the flat die extrusions was close to this value.

Figure 4.3 displays the radial strain in the samples extruded with a flat die as a function of position along the wire.

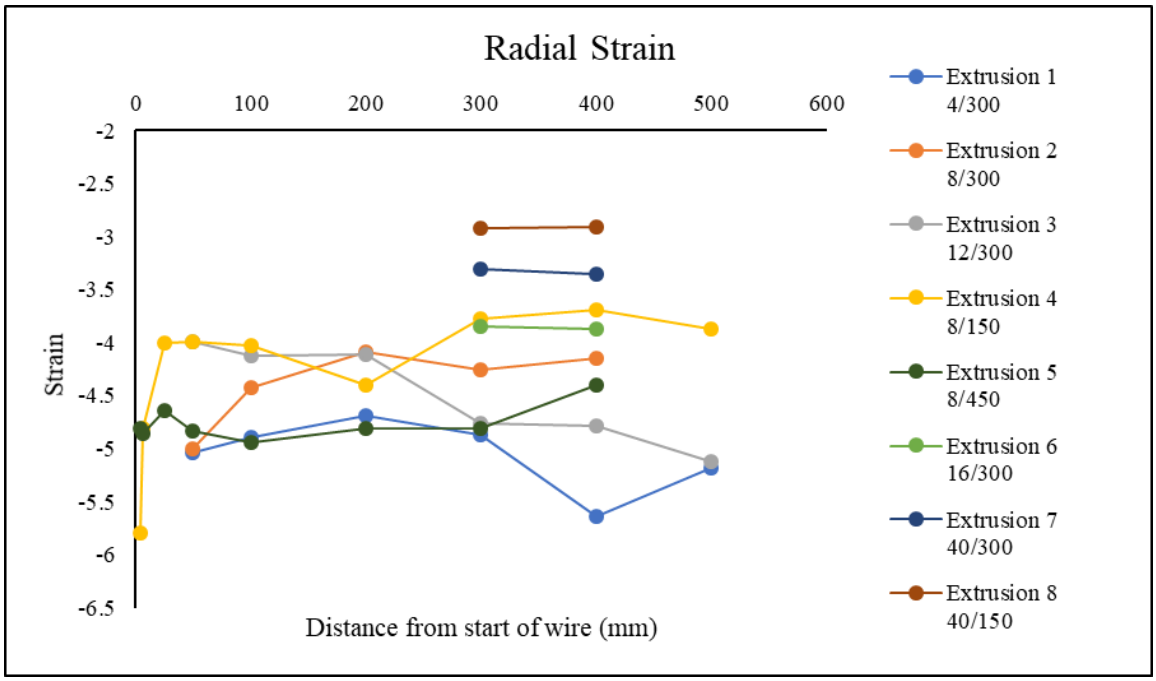

Figure 4.3: Radial strain in flat die wires as a function of position from the start of the extrusion.

The radial strain shows a transient region near the start of the wires, similar to the longitudinal strain. After approximately 100 mm the values of radial strain remain constant throughout the extrusion. The radial strain varied from wire to wire, showing that it is affected by the selected extrusion parameters. The expected radial strain value for a 10:1 conventional extrusion is -2.3. The radial strain in all the friction stir extruded wires was significantly lower than this expected value.

Figure 4.4 displays the circumferential strain in the flat die samples as a function of position along the wire.

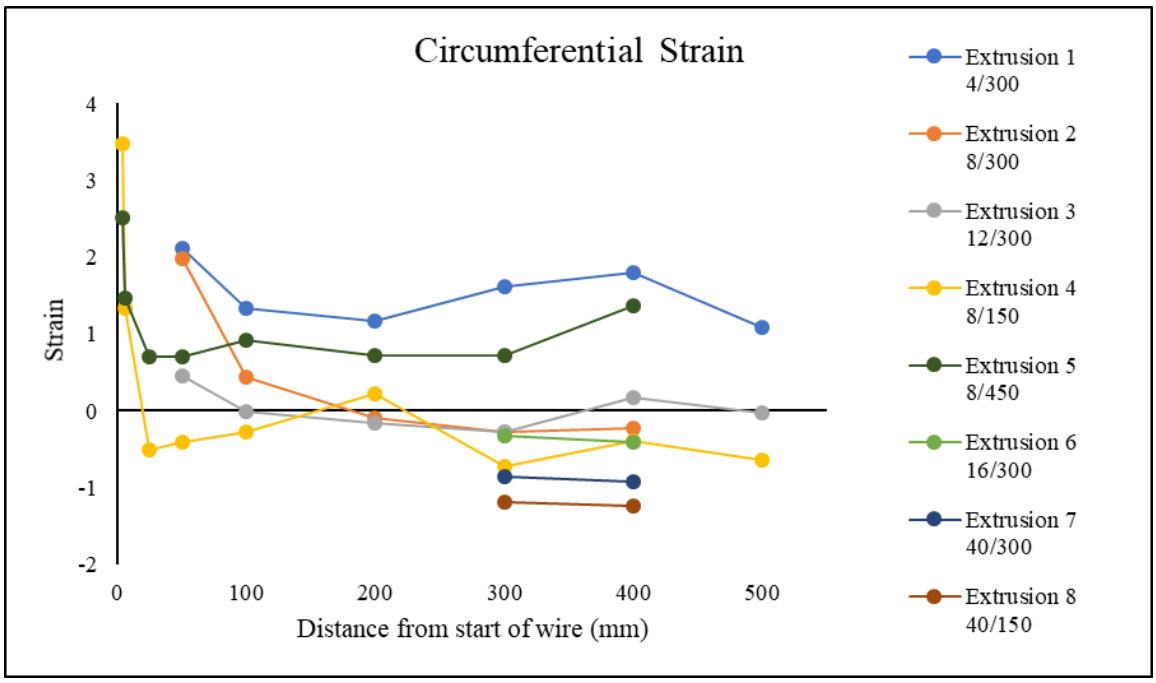

Figure 4.4: Theta strain in flat die wires as a function of position from the start of the extrusion.

The circumferential strain results show a similar transient region at the beginning of the extrusion. After this region the circumferential strain remained steady for the rest of the length of the wire. Similar to the radial strain results, the different extrusion parameters did produce different circumferential strain values. While the circumferential strain varied from wire to wire, all recorded values were significantly higher than -2.3, the circumferential strain expected in conventional extrusion with a 10:1 reduction ratio.

4.3 EFFECT OF PARAMTERES ON STRAIN

In order to analyze the effect of the die advance rate, wires that were extruded with the same rotational speed but different die advance rates are compared. The only factor changing between these wires is the die advance rate used, so the difference in strain results can be attributed to this change in die advance rate. Figure 4.5 displays strain data from the 5 wires extruded with a rotational speed of 300 rpm and die advance rates varying from 4

mm/min to 40 mm/min. The average value of each of the 3 strain components is plotted against the die advance rate used for each extrusion.

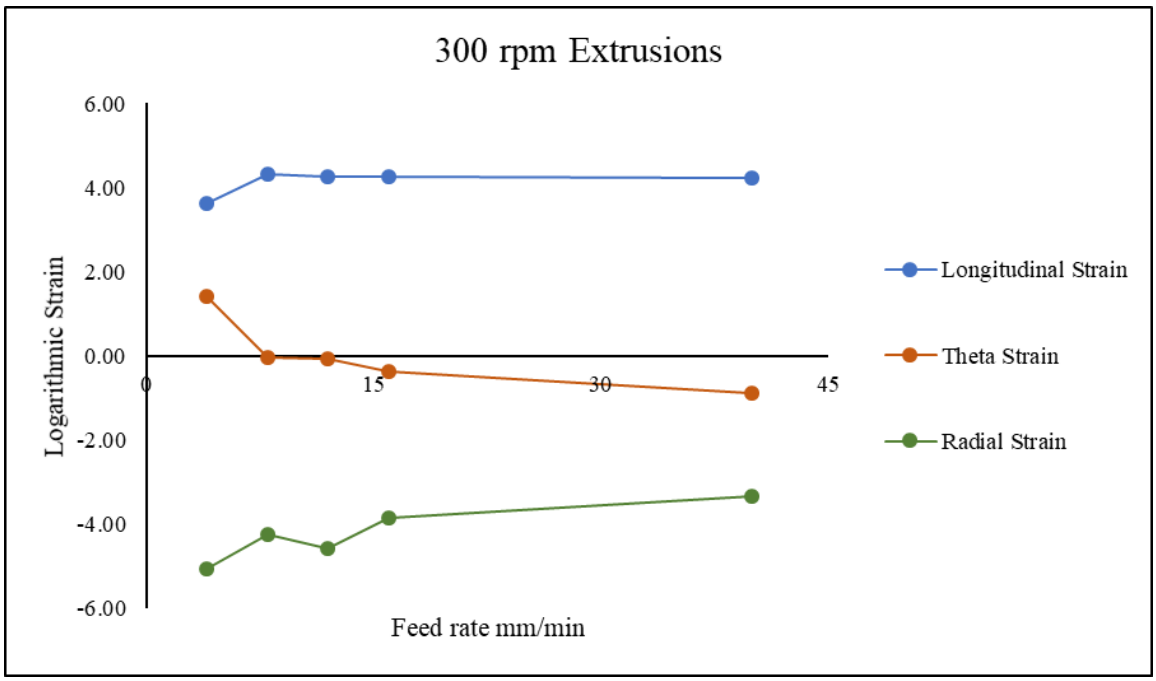

Figure 4.5: The average strain values of wires extruded with a rotational speed of 300 rpm plotted against the die advance rate used for each extrusion.

As expected, the longitudinal strain remains constant and is not affected by the different feed rates. As the feed rate increases, the circumferential strain decreases and the radial strain increases. An increase in feed rate causes both the circumferential and radial strain to move closer to -2.6, the expected value in a conventual extrusion.

In order to analyze the effect of rotational speed, wires with the same feed rate and different rotational speeds are compared. There are two groups of wires produced at the same feed rate and different rotational speeds. First, fig. 4.6 displays the average strain data from three wires extruded with a constant feed rate of 8 mm/min plotted against the rotational speed each wire was extruded with. The rotational speeds used to extrude these wires are 150 rpm, 300 rpm, and 450 rpm. Second, fig. 4.7 displays the average strain data

from the two wires extruded with a feed rate of 40 mm/min. These wires were extruded with rotational speeds of 150 rpm and 300 rpm.

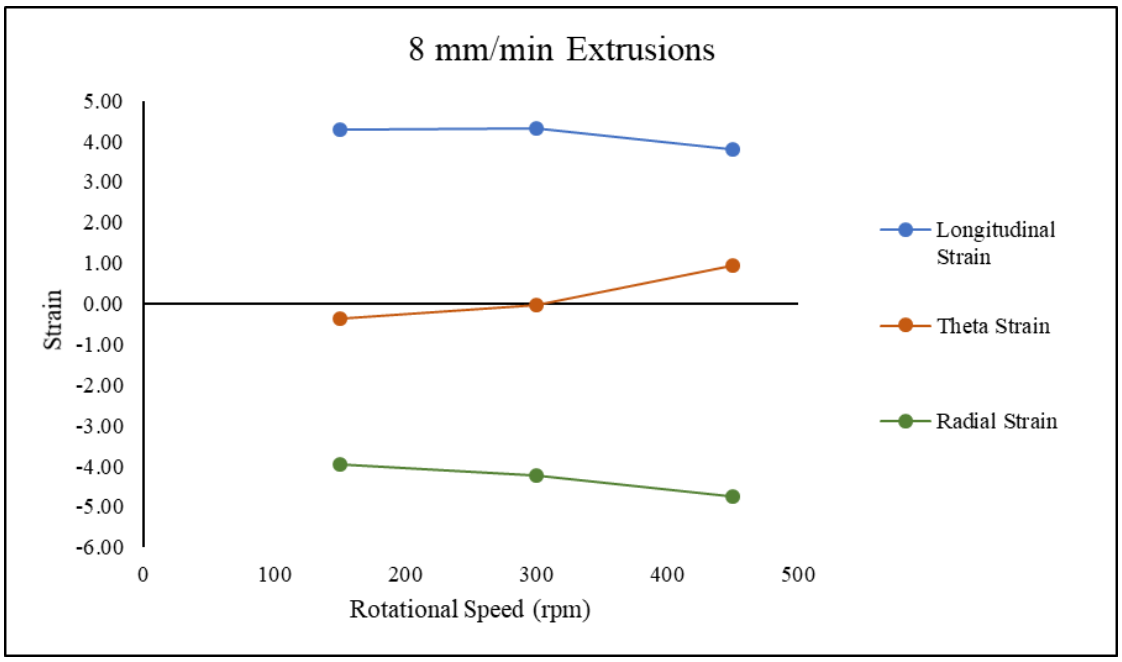

Figure 4.6: The average strain values of wires extruded with an 8 mm/min feed rate plotted against the rotational speed used for each extrusion.

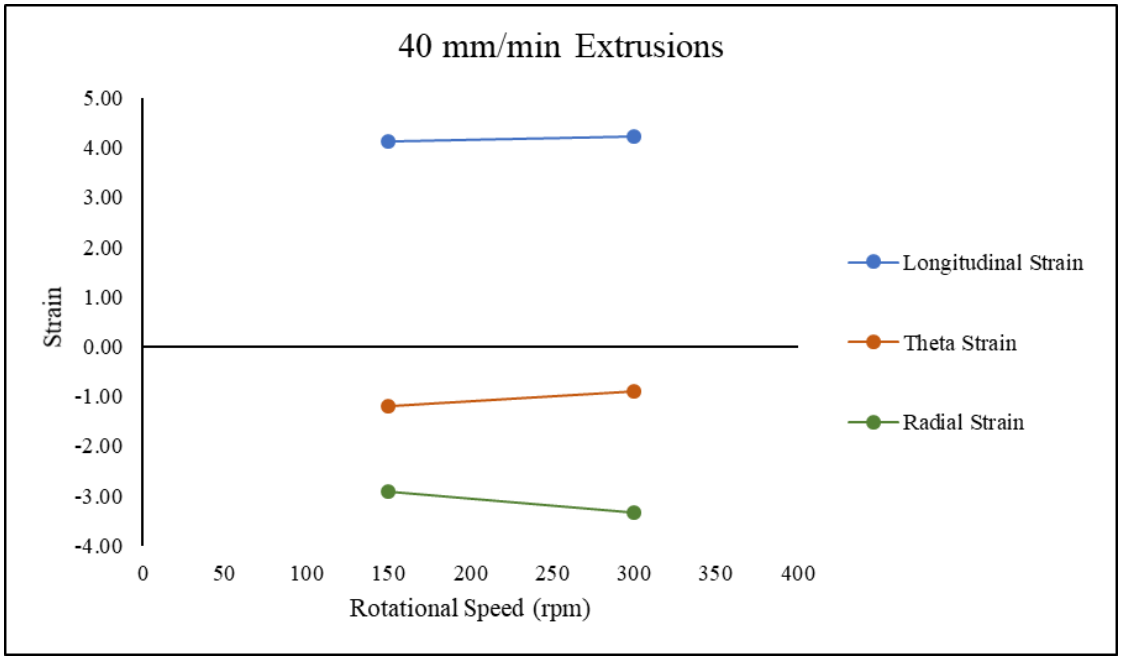

Figure 4.7: The average strain values of wires extruded with a 40mm/min feed rate plotted against the rotational speed used for each extrusion.

The extrusions at 8 mm/min and 40 mm/min show similar trends when it comes to the effect of rotational speed. Higher rotational speeds lead to a decrease in radial strain and an increase in circumferential strain. As rotational speed is decreased, the values of radial strain and circumferential strain move closer to the expected value in a conventional 10:1 extrusion.

In order to evaluate the overall effects of the extrusion parameters, the strain results for each wire are correlated to the die advance per revolution of the wire. The die advance per revolution takes into account both the feed rate and the rotational speed used. The die advance per revolution for each wire are displayed in table 4.1.

Table 4.1: Die advance per revolution for each wire

Wire	Die Advance Rate	Die Rotation Rate	Die Advance per Revolution
1	4 mm/min	300 rpm	0.0133 mm/rev
2	8 mm/min	300 rpm	0.0266 mm/rev
3	12 mm/min	300 rpm	0.04 mm/rev
4	8 mm/min	150 rpm	0.0533 mm/rev
5	8 mm/min	450 rpm	0.0177 mm/rev
6	16 mm/min	300 rpm	0.0533 mm/rev
7	40 mm/min	300 rpm	0.1333 mm/rev
8	40 mm/min	150 rpm	0.2667 mm/rev

Figure 4.8 shows the average value for each component of strain as a function of DAPR.

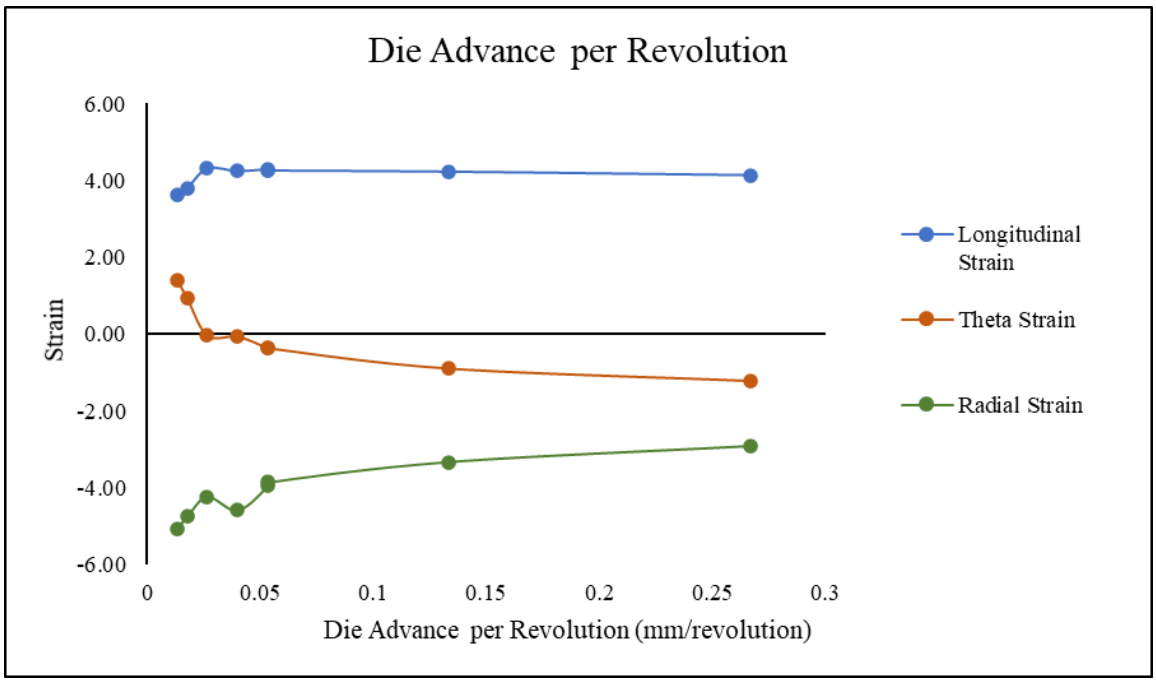

Figure 4.8: Average strain values as a function of die advance per revolution

As seen previously, longitudinal strain remains relatively constant and is not affected by the changing extrusion parameters. As the die advance per revolution becomes larger, the theta strain decreases and the radial strain increases. These strain values are furthest from each other and furthest from the expected value in conventional extrusion with lower DAPR. As the DAPR is increases, the radial and theta strains begin to converge on the expected conventional extrusion values. In a conventual extrusion the die does not rotate, causing the DAPR for a conventual extrusion to be infinite. Therefore, as the DAPR of a friction stir extrusion increases, it becomes more similar to conventional extrusion. This is supported by the strain results because as the DAPR increases and the extrusion become more like a conventional extrusion, the strain values converge on the strain values of the conventional extrusion.

Extrusions 4 and 6 have the same die advance per revolution but have different process parameters. Wire 6 was extruded with a rotational speed of 300 rpm and a feed rate

of 16 mm/min while wire 4 was extruded with a rotational speed of 150 rpm and a feed rate of 8 mm/min. While these process parameters are significantly different, the DAPR for both extrusions was 0.0533 mm/revolution. The strain components for both wires are displayed in fig. 4.9 as a function of the position from the start of the extrusion.

Despite the fact that these two wires were produced at different rotational speeds and feed rates, the strain results are very similar. This shows the strain response is controlled by the ratio of the feed rate to the rotational speed rather than the individual values of each parameter.

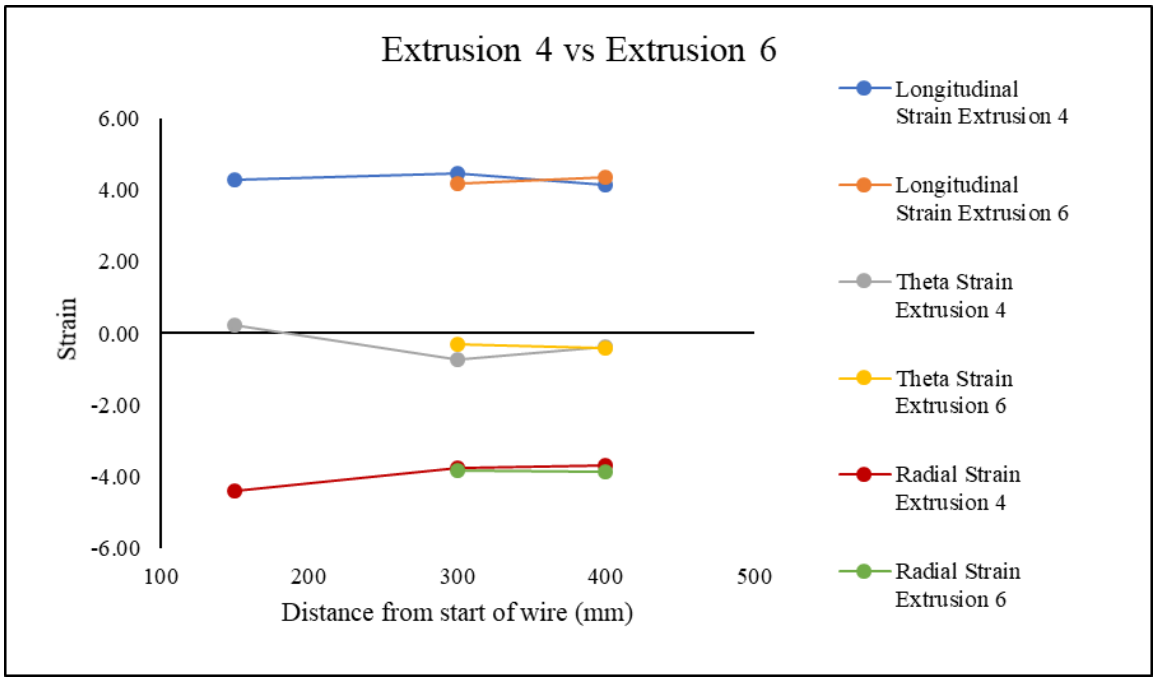

Figure 4.9: The strain components of extrusion 4 and extrusion 6 as a function of distance from the start of the extrusion.

4.4 SCROLL FACE DIE

In order to see the effect of die geometry, extrusions were performed with a scroll die with the same parameter combinations used for the flat die extrusions. Figures 4.10 through 4.12 compare cross sections from wires extruded with the same rotational speed

and feed rate but with different dies. All the images in figures 4.10 through 4.12 are from cross sections taken 300 mm from the start of the extrusion.

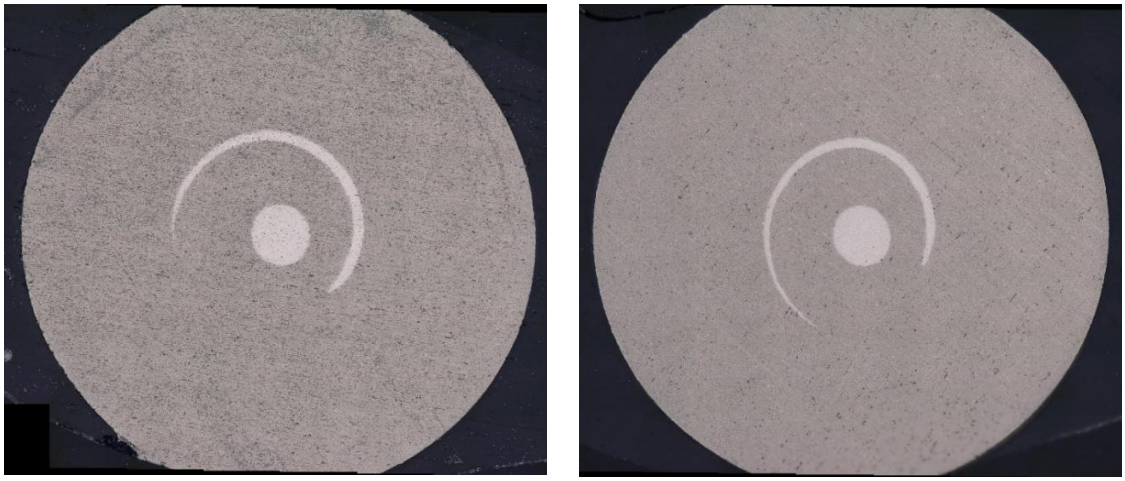

(a) (b)

Figure 4.10: Cross sections from extrusions performed at 300 rpm and 16 mm/min. (a) flat die extrusion. (b) scroll die extrusion

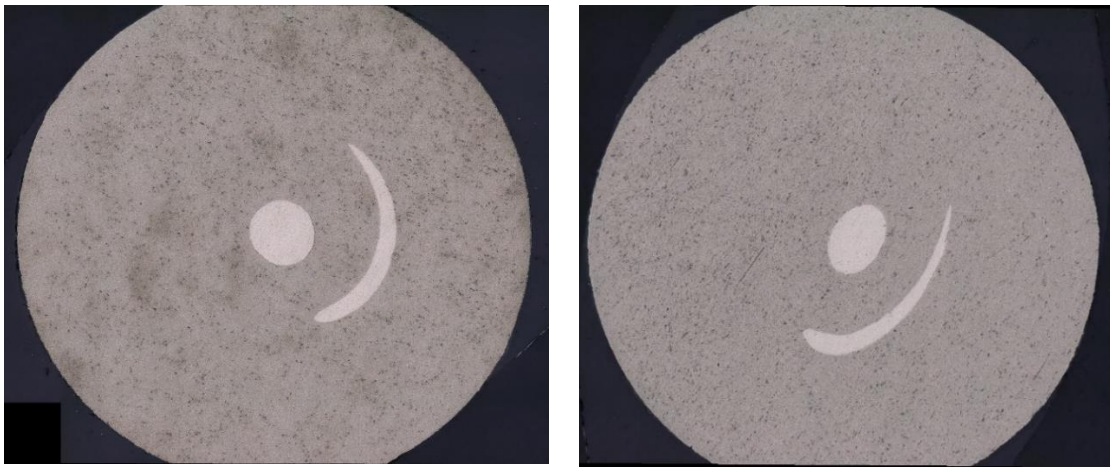

(a) (b)

Figure 4.11: Cross sections from extrusions performed at 300 rpm and 40 mm/min. (a) flat die extrusion. (b) scroll die extrusion

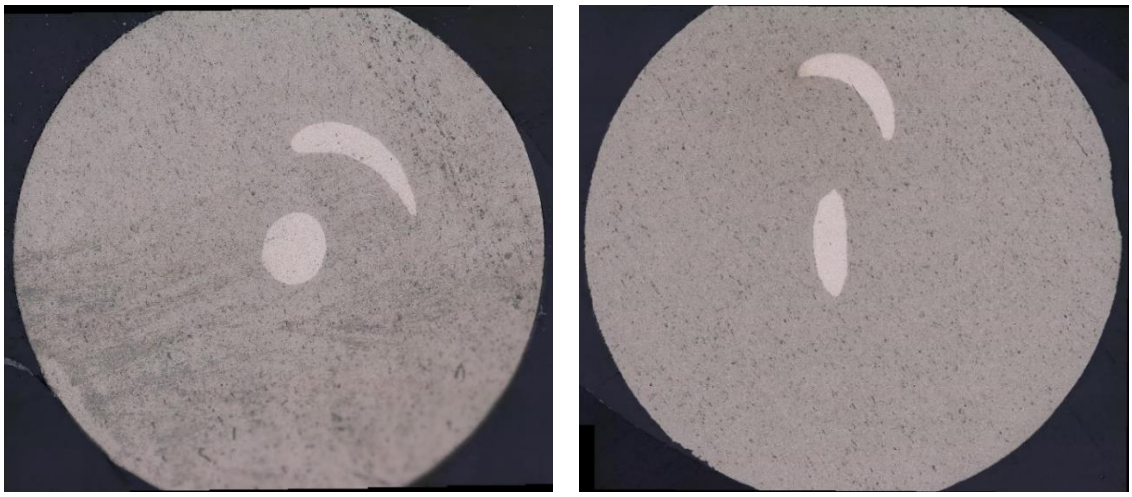

(a) (b)

Figure 4.12: Cross sections from extrusions performed at 150 rpm and 40 mm/min. (a) flat die extrusion. (b) scroll die extrusion

The marker wire in the flat die samples remained circular while the center and 1/3r marker wires showed an oval pattern in multiple scroll die samples. This oval pattern was consistent across all the cross sections from these scroll die samples. This shows that the die geometry did influence the pattern of material flow throughout the process. To determine the influence of die geometry on strain, the three strain components were calculated for the scroll die samples, and the results are displayed in figures 4.13 through 4.15.

In order to determine the effect of die geometry, the strains of the flat die wires were directly compared to the strains in the scroll die wires extruded under the same conditions. Figure 4.16 compares the strain components of the 2 wires extruded with a rotational speed of 300 rpm and a feed rate of 40 mm/min.

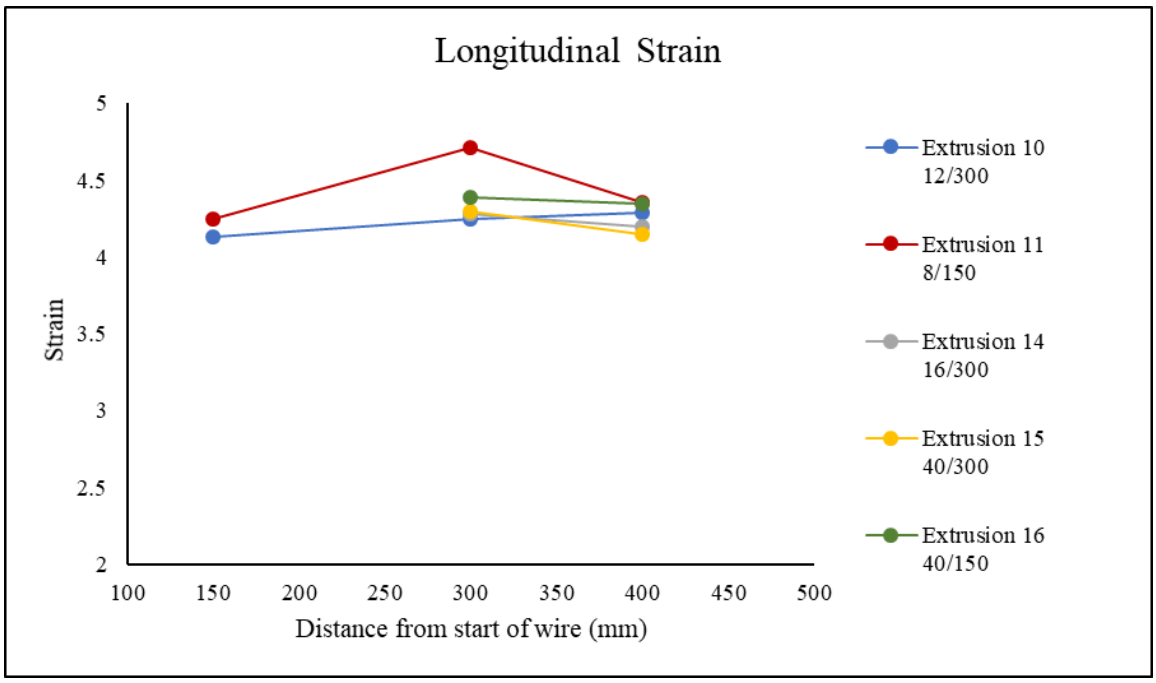

Figure 4.13: Longitudinal strain in the scroll die samples as a function of distance from the start of the extrusion.

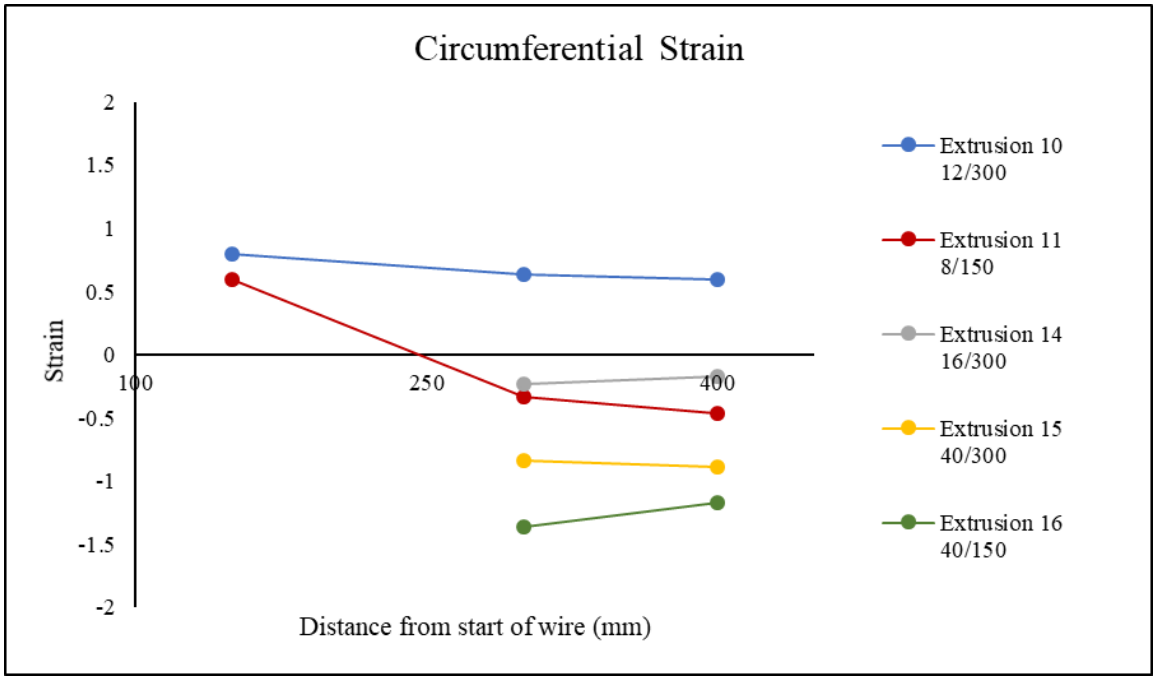

Figure 4.14: Theta strain in the scroll die samples as a function of distance from the start of the extrusion.

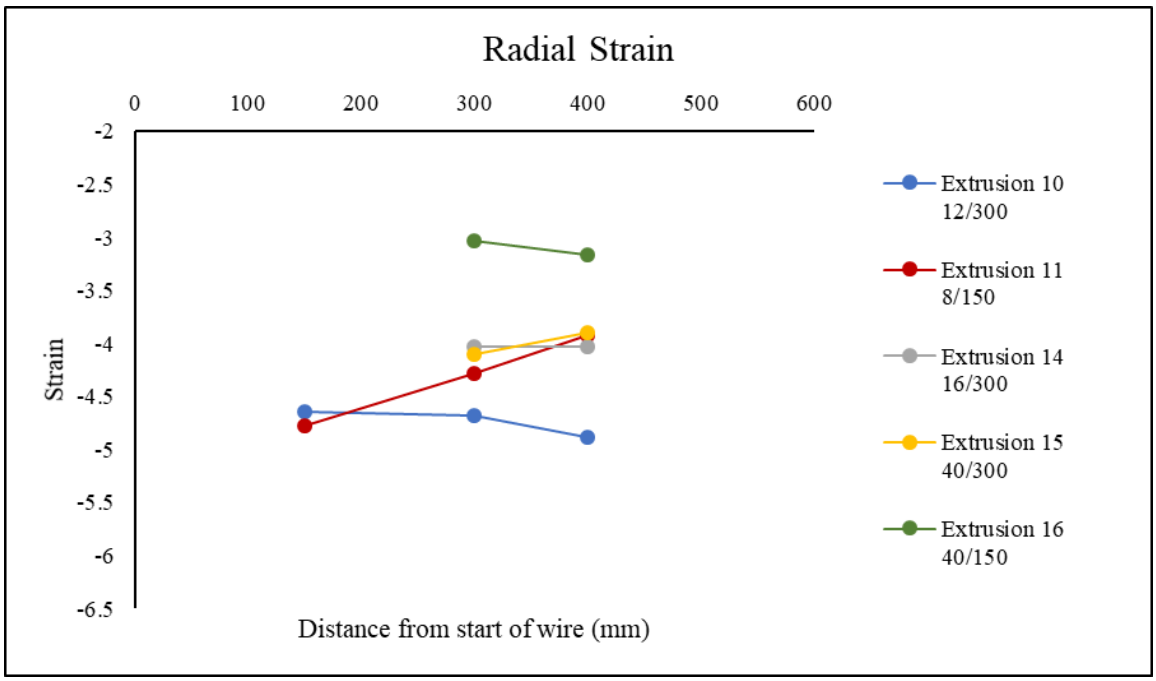

Figure 4.15: Radial strain in the scroll die samples as a function of distance from the start of the extrusion.

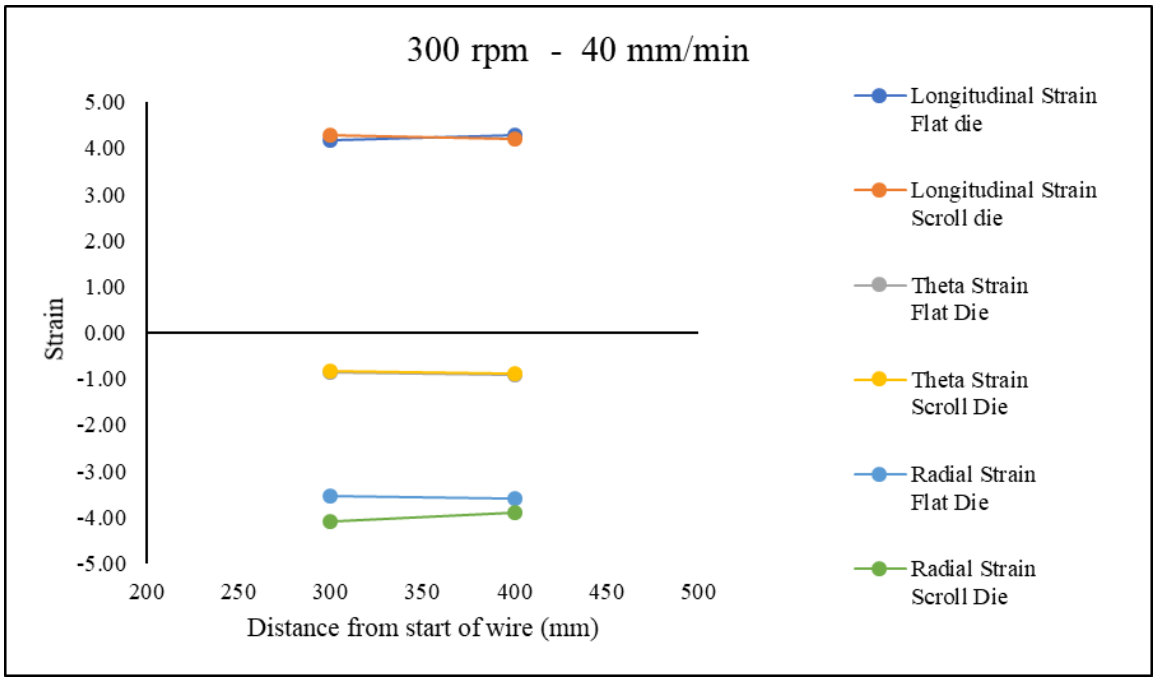

Figure 4.16: Strain Components of wires extruded at 300 rpm and 40 mm/min with both a flat die and scroll die as a function of distance from the start of the extrusion.

Figure 4.17 compares the strain components of the 2 wires extruded with a rotational speed of 150 rpm and a feed rate of 40 mm/min. Figure 4.18 compares the strain components of the 2 wires extruded with a rotational speed of 300 rpm and a feed rate of 12 mm/min. Figure 4.19 compares the strain components of the 2 wires extruded with a rotational speed of 150 rpm and a feed rate of 8 mm/min.

Figures 4.16 through 4.19 show that the longitudinal, circumferential, and radial strains were very similar between the flat die and scrolled die wires. While the die geometry did change the material flow pattern it did not have significant impact on the strain components.

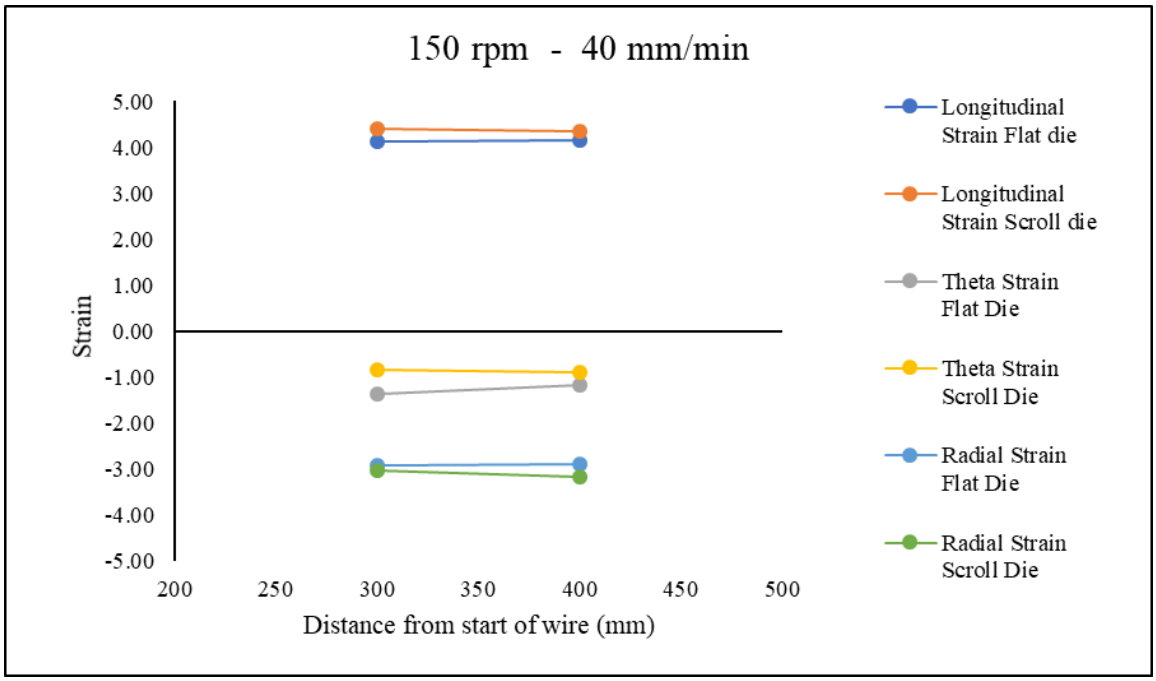

Figure 4.17: Strain Components of wires extruded at 150 rpm and 40 mm/min with both a flat die and scroll die as a function of distance from the start of the extrusion.

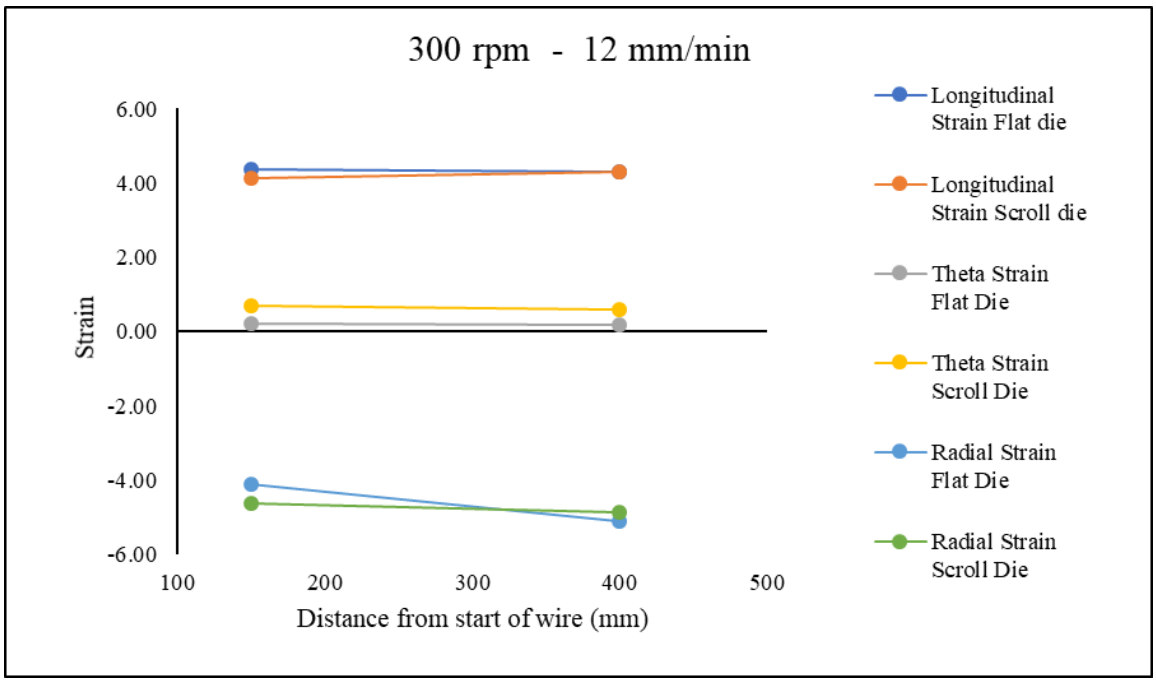

Figure 4.18: Strain Components of wires extruded at 300 rpm and 12 mm/min with both a flat die and scroll die as a function of distance from the start of the extrusion.

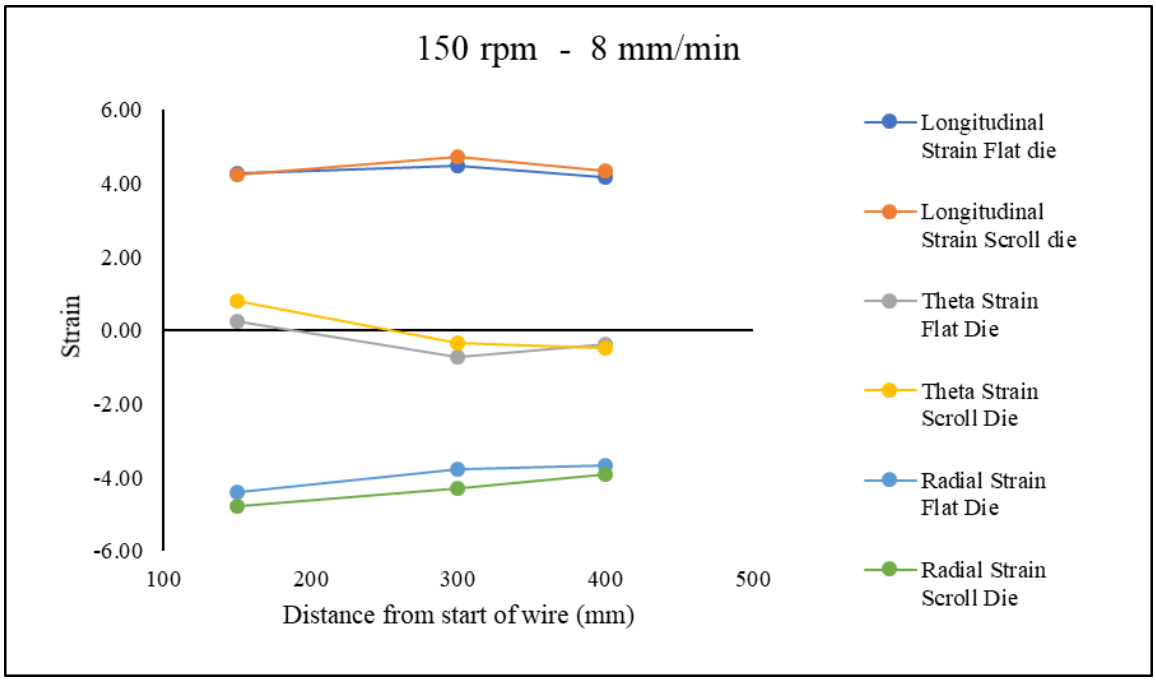

Figure 4.19: Strain Components of wires extruded at 150 rpm and 8 mm/min with both a flat die and scroll die as a function of distance from the start of the extrusion.

4.5 VALIDITY OF METHOD

In order to verify the accuracy of the method used to calculate strain, the sum of the strain components was analyzed. Friction extrusion is a plastic deformation process with a constant volume, and therefore the sum of any three mutually perpendicular strain components should be zero [24]. The sum of the strain values are displayed in fig. 4.20.

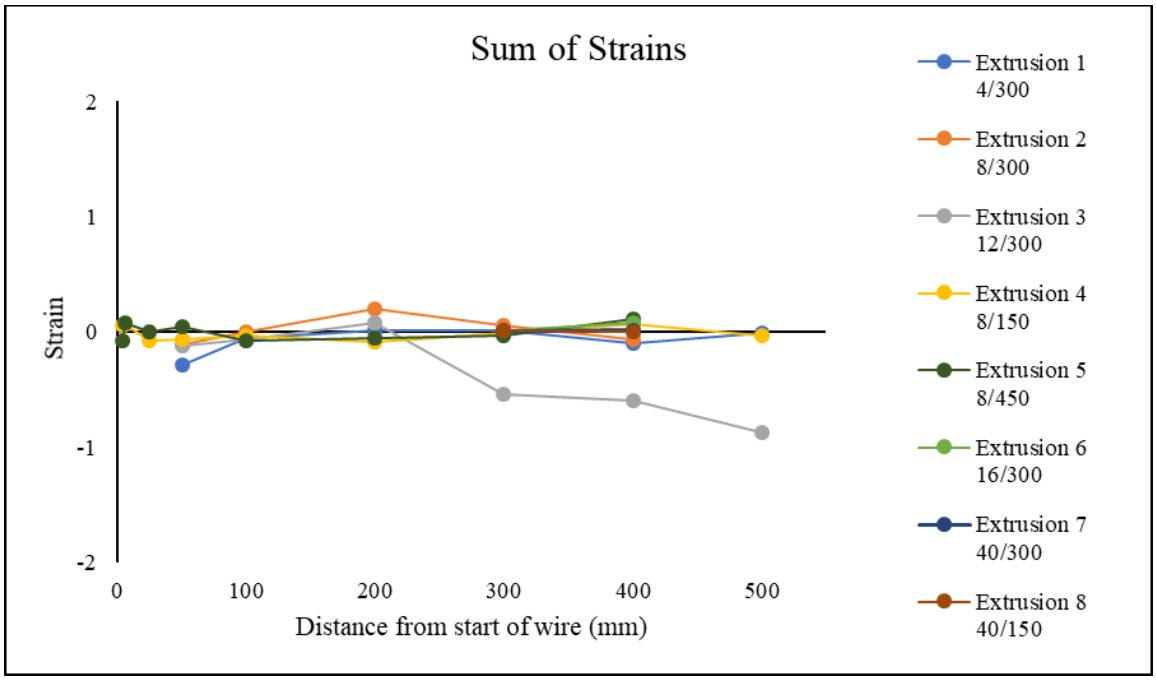

Figure 4.20: The sum of the strain components plotted against the distance from the start of wire for all extrusions.

With the exception of extrusion 3, the sum of the strain components were very close to zero. This shows that the method used to calculate the strain components produced reliable results.

CHAPTER 5

CONCLUSIONS

1. The sum of the strain components was very close to zero for all wires, which is expected in a controlled volume plastic deformation process. This shows that the method used produced accurate strain results.

2. The longitudinal strain is not dependent on the extrusion parameters and is similar to the longitudinal strain expected in a conventional extrusion with the same reduction ratio.

3. The radial and circumferential strains are dependent on the extrusion parameters. As the DAPR increases, the extrusion becomes more similar to conventual extrusion and the radial and circumneutral strain components converge on the expected value in a conventional extrusion.

4. The strain response is controlled by the ratio of the die advance rate to the rotational speed rather than the individual values of each parameter.

5. While the die geometry affected the pattern of the marker wire, the scroll die samples showed very similar strain values to the flat die samples produced with equivalent process parameters.

REFERENCES

[1] Thomas, WM, ED Nicholas, and SW Kalle. “Friction Stir Welding and Processing.” *The Minerals, Metals & Material Society*, 2001.

[2] Nicholas, E. D. “Friction Processing Technologies.” *Welding in the World*, vol. 47, no. 11-12, 2003, pp. 2–9., doi:10.1007/bf03266402.

[3] Abu-Farha, Fadi. “A Preliminary Study on the Feasibility of Friction Stir Back Extrusion.” *Scripta Materialia*, vol. 66, no. 9, 2012, pp. 615–618., doi:10.1016/j.scriptamat.2012.01.059.

[4] W. M. Thomas, E. D. Nicholas, J. C. Needham, M. G. Murch, P. Templesmith, and C. J. Dawes, “GB Patent application no. 9125978.8,” Int. Pat. Appl. No PCTGB9202203, 1991.

[5] Baffari, Dario, Anthony P. Reynolds, Attilio Masnata, Livan Fratini, and Giuseppe Ingarao. “Friction Stir Extrusion to Recycle Aluminum Alloys Scraps: Energy Efficiency Characterization.” *Journal of Manufacturing Processes*, vol. 43, 2019, pp. 63–69., doi:10.1016/j.jmapro.2019.03.049.

[6] Ingarao, Giuseppe, Dario Baffari, Ellen Bracquene, Livan Fratini, and Joost Duflou. “Energy Demand Reduction Of Aluminum Alloys Recycling Through Friction Stir Extrusion Processes Implementation.” *Procedia Manufacturing*, vol. 33, 2019, pp. 632–638., doi:10.1016/j.promfg.2019.04.079.

[7] Kondoh, Katsuyoshi, Tachai Luangvaranunt, and Tatsuhiko Aizawa. “Solid-State Recycling of AZ91D Magnesium Alloy Chips.” *Journal of Japan Institute of Light Metals*, vol. 51, no. 10, 2001, pp. 516–520., doi:10.2464/jilm.51.516.

[8] Ansari, Mohammad Ali, Mohammad Kazem Besharati Givi, Reza Abdi Behnagh, and Morteza Narvan. “Solid-State Production of Micro-Engineered Advanced Wire from Magnesium Chips by Friction Stir Extrusion.” *Annual International Conference on Mechanical Engineering-ISME2015,* Apr. 2015, doi:10.13140/2.1.2784.3364.

[9] Buffa, Gianluca, Davide Campanella, Livan Fratini, and Fabrizio Micari. "AZ31 Magnesium Alloy Recycling through Friction Stir Extrusion Process." *International Journal of Material Forming* 9.5 (2015): 613-18., doi:10.1007/s12289-015-1247-6.

[10] Tang, W., and A.p. Reynolds. “Production of Wire via Friction Extrusion of Aluminum Alloy Machining Chips.” *Journal of Materials Processing Technology*, vol. 210, no. 15, 2010, pp. 2231–2237., doi:10.1016/j.jmatprotec.2010.08.010.

[11] Behnagh, Reza Abdi, Ramezanali Mahdavinejad, Amin Yavari, Masoud Abdollahi, and Morteza Narvan. “Production of Wire From AA7277 Aluminum Chips via Friction-Stir Extrusion (FSE).” *Metallurgical and Materials Transactions B*, vol. 45, no. 4, 2014, pp. 1484–1489., doi:10.1007/s11663-014-0067-2.

[12] Whalen, Scott, Matthew Olszta, Christian Roach, Jens Darsell, Daniel Graff, Md. Reza-E-Rabby, Timothy Roosendaal, Wayne Daye, Tom Pelletiers, Suveen Mathaudhu, and Nicole Overman. “High Ductility Aluminum Alloy Made from

Powder by Friction Extrusion." *Materialia*, vol. 6, 2019, p. 100260., doi:10.1016/j.mtla.2019.100260.

[13] Baffari, Dario, Gianluca Buffa, Davide Campanella, and Livan Fratini. "Al-SiC Metal Matrix Composite Production through Friction Stir Extrusion of Aluminum Chips." *Procedia Engineering*, vol. 207, 2017, pp. 419–424., doi:10.1016/j.proeng.2017.10.798.

[14] Baffari, Dario, Anthony P. Reynolds, Xiao Li, and Livan Fratini. "Influence of Processing Parameters and Initial Temper on Friction Stir Extrusion of 2050 Aluminum Alloy." *Journal of Manufacturing Processes*, vol. 28, 2017, pp. 319–325., doi:10.1016/j.jmapro.2017.06.013.

[15] Ahmad Khanbeigi, Masoud, Ghader Faraji, and O. Shapourgan. "Microstructure and Mechanical Properties of Al Tube Processed by Friction Stir Tube Back Extrusion (FSTBE)." *Transactions of the Indian Institute of Metals*, vol. 70, 2017, pp. 1849–1856., doi:10.1007/s12666-016-0987-4.

[16] Behnagh, Reza Abdi, Ninggang Shen, Mohammad Ali Ansari, Morteza Narvan, Mohammad Kazem Besharati Givi, and Hongtao Ding. "Experimental Analysis and Microstructure Modeling of Friction Stir Extrusion of Magnesium Chips." *Journal of Manufacturing Science and Engineering*, vol. 138, no. 4, 2015, doi:10.1115/1.4031281.

[17] Sharifzadeh, Mohammad, Mohammad Ali Ansari, Morteza Narvan, Reza Abdi Behnagh, Alireza Araee, and Mohammad Kazem Besharati Givi. "Evaluation of Wear and Corrosion Resistance of Pure Mg Wire Produced by Friction Stir

Extrusion." *Transactions of Nonferrous Metals Society of China*, vol. 25, no. 6, 2015, pp. 1847–1855., doi:10.1016/s1003-6326(15)63791-8.

[18] Valberg , Henry. "Metal Flow in the Direct Axisymmetric Extrusion of Aluminum." *Journal of Material Processing Technology*, vol. 31, 1992, pp. 39–55.

[19] Seidel, T.U., and A.P. Reynolds. "Visualization of the Material Flow in AA 2195 Friction-Stir Welds Using a Marker Insert Technique." *Metallurgical and Materials Transactions* , Nov. 2001, pp. 2879–2884.

[20] Baffari, Dario, Gianluca Buffa, Davide Campanella, Livan Fratini, and Anthony P. Reynolds. "Process Mechanics in Friction Stir Extrusion of Magnesium Alloys Chips through Experiments and Numerical Simulation." *Journal of Manufacturing Processes*, vol. 29, 2017, pp. 41–49., doi:10.1016/j.jmapro.2017.07.010.

[21] Li, X., W. Tang, and A. P. Reynolds. "Material Flow and Texture in Friction Extruded Wire." *Friction Stir Welding and Processing VII*, 2013, pp. 339–347., doi:10.1002/9781118658345.ch35.

[22] Li, X., W. Tang, A.p. Reynolds, W.a. Tayon, and C.a. Brice. "Strain and Texture in Friction Extrusion of Aluminum Wire." *Journal of Materials Processing Technology*, vol. 229, 2016, pp. 191–198., doi:10.1016/j.jmatprotec.2015.09.012.

[23] Qamar, S.Z. "FEM Study of Extrusion Complexity and Dead Metal Zone ." *Archives of Material Science and Engneering*, vol. 36, no. 2, Apr. 2009, pp. 110–117.

[24] Boresi, Arthur P., and Richard J. Schmidt. *Advanced Mechanics of Materials*. 6th ed., John Wiley & Sons, Inc., 2003.